

State-Sensitive Monitoring of Active and Promoter Sites. Applications to Au/Titania and Pt-Sn/Silica Catalysts by XAFS Combined with X-Ray Fluorescence Spectrometry[#]

Yasuo Izumi,[†] Dilshad Masih,[†] Jean-Pierre Candy,[‡] Hideaki Yoshitake,[¶]
Yasuko Terada,[§] Hajime Tanida,[§] and Tomoya Uruga[§]

[†] Interdisciplinary Graduate School of Science and Engineering, Tokyo Institute of Technology, 4259 Nagatsuta, Midori-ku, Yokohama 226-8502, Japan, [‡] LCOMS-CPE, 43 bd du 11 Novembre 1918, 69616 Villeurbanne, France, [¶] Graduate School of Engineering, Yokohama National University, Tokiwadai, Hodogaya-ku, Yokohama 240-8501, Japan, and [§] JASRI, Kohto 1-1-1, Sayo 679-5198, Japan

Abstract. State-sensitive XAFS was enabled combined with high-energy-resolution ($\Delta E = 0.3$ eV @ 5.5 keV) X-ray fluorescence spectrometry and applied to Au sites of Au/TiO₂ and Sn promoter sites of Pt-Sn/SiO₂. Each state of interfacial Au sites located on Ti/O atoms and negatively/positively charged Au_n clusters was discriminated. Feasibility of more direct information of on-site catalysis via frontier orbital-sensitive XAFS was demonstrated.

Keywords: XAFS, fluorescence spectrometry, state sensitive, site selective, catalyst, gold, tin, frontier orbital
PACS: 61.10.Ht, 78.70.Dm, 78.70.En, 82.45.Jn, 82.65.+r

INTRODUCTION

X-ray absorption fine structure is able to pick up active/promoter sites of catalysts. During catalytic processes, dynamic state transformation of these sites is taking place. Therefore, state-sensitive monitoring of XAFS gives direct information of the catalytic role. In this work, XAFS combined with high-energy-resolution X-ray fluorescence spectrometry [1,2] was applied for state-sensitive measurements to detect heterogeneity of Au clusters (average particle size 9.2 ± 1.4 nm, Figure 1) on TiO₂. Catalytic importance of perimeter sites, step edge sites, and extra electrons on TiO₂ support was suggested [3]. To enable narrower size distribution and higher loading of Au clusters, mesoporous TiO₂ (specific SA 1200 m²g⁻¹) was used. In addition, better-resolved, steeper XANES spectra were obtained to remove the core-hole lifetime width (I) of Au L₃ and Sn K levels to identify the Sn occupation site on Pt/silica.

METHODS

The Au/TiO₂ catalyst was prepared by mixing HAuCl₄·4H₂O (1.3 mM, 25.0 ml) [4] with mesoporous TiO₂ (0.50 g) [5] at constant pH 8 followed by calcination at 523 K. The Pt-Sn/SiO₂

catalyst (2.5 wt% Pt, Sn/Pt atomic ratio 1.0) was prepared as in ref. 6.

X-ray measurements were performed at beamline 37XU of SPring-8. The storage ring energy was 8.0 GeV operated in top-up mode (ring current 99 – 97 mA). A Si(111) monochromator and Rh-coated mirror were used. The combination of X-ray beam position monitoring [7] and monochromator stabilization [8] minimized the deviation of beam position at the sample. Sn and V data were measured at beamline 10XU [6] and KEK-PF 9C, respectively.

Ge(555), (13,13,13), and (422) reflections were used for Au L α_1 , Sn K α_1 , and V K $\beta_{5,2}$ detection, respectively. The slit opening in front of I₀ ion chamber was 1.0 mm(V)×0.5 mm(H). The sample was set in a nearly horizontal plane. Both sample and SC were covered with lead box of ≈ 3 mm thickness except for in the beam paths.

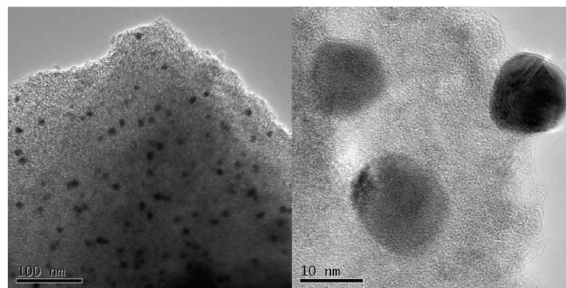


FIGURE 1. HR FE-TEM images for Au/mesoporous-TiO₂ (JEM-2010F; CAMA, Tokyo Inst. Tech.).

[#] This paper is part 19 in the series.

X-ray spectra were measured at 290 K. Au $L\alpha_1$, Sn $K\alpha_1$, and V $K\beta_{5,2}$ emission spectra were measured. Then, the fluorescence spectrometer was tuned and state-sensitive XAFS spectra were measured. The undulator gap (SPRING-8) was optimized to maximize the beam flux at each data point.

RESULTS

Au State-Sensitive Measurements for Au/Mesoporous-TiO₂ Catalysts

Au $L\alpha_1$ emission spectra were measured for Au/mesoporous-TiO₂ (Figure 2a). When the excitation energy (E_{exc}) was between 11922.0 and 11948.6 eV, the peak energy and intensity changed negligibly (9713.0–9713.3 eV, (3)–(1)). When the E_{exc} value decreased to 11919.1 eV, the peak shifted downward to 9711.0 eV and the intensity decreased to 66% (4).

Corresponding to the emission peaks in (1)–(3), state-sensitive Au L_3 -edge absorption spectra were measured (Figure 2b). When tuned to 9713.0 eV (emission peak top), the obtained spectrum (3, dots) was similar to the one measured for Au metal (3, line). The Au $L\alpha_1$ -detecting XANES was sharper because the energy resolution (3.3 eV) was smaller than the Γ value for Au L_3 (5.41 eV) [6,9].

When the spectrometer was tuned to 9707.6 eV ($\Delta = -5.4$ eV), the obtained spectrum 1 shifted by -3.5 eV from spectrum 3. This negative shift of XANES corresponded to the emission peak shift to 9711.0 eV (Figure 2a-4). When the spectrometer was tuned to 9719.7 eV ($\Delta = +6.7$ eV), the obtained spectrum 4 shifted by $+4.4$ eV from spectrum 3. Alternatively, spectrum 4 was similar to that for Au^ICl(PPh₃) (Figure 3b).

The peak intensity just above the absorption edge varied depending on the fluorescence tune energy. The peak at 11924.1 eV in Figure 2b-3 was most intense among the four absorption spectra. This feature corresponded to the theoretical XANES spectrum generated by FEFF8.1 [10] for interfacial Au atom sites located on Ti atoms (Figures 3c and 4a). Charge may transfer from Au 5d to form Ti³⁺ states at the interface [11]. The peak was not resolved from the absorption edge for interfacial Au atom sites located on O atom (Figures 3d and 4b) [12–14], similar to Figure 2b-1 or 2b-2.

In summary, interfacial Au sites located on Ti (Figure 2b-3) and on O (2b-2) and Au^{≈1+}_n [13] and Au^{x-}_n clusters [3] on amorphous TiO₂ (Figures 2b-4 and 2b-1, respectively) were extracted using state-sensitive Au L_3 -edge XAFS.

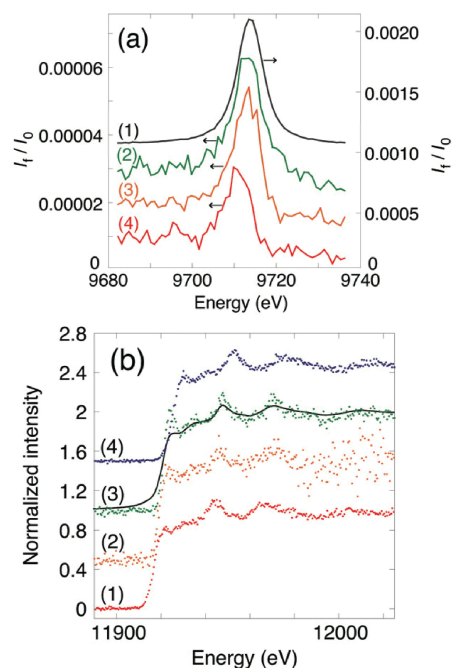


FIGURE 2. (a) Au $L\alpha_1$ emission spectra for Au/mesoporous-TiO₂ with the excitation energy set to 11948.6 (1), 11934.1 (2), 11922.0 (3), and 11919.1 eV (4). The vertical opening of the receiving slit for spectrum 1 was 16 times greater than in other cases. (b) Au L_3 -edge XANES (dots) measured tuning the fluorescence spectrometer to 9707.6 (1), 9710.4 (2), 9713.0 (3), and 9719.7 eV (4). Reference spectrum for Au metal was also plotted as line (3).

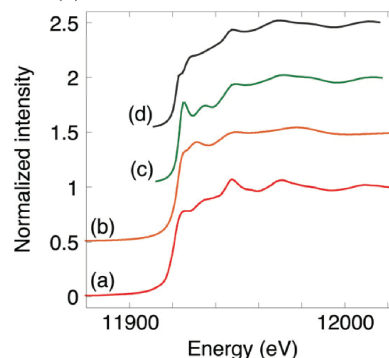


FIGURE 3. Au L_3 -edge XANES spectra for Au metal (a), Au^ICl(PPh₃) (b), and interfacial Au sites located on Ti and O atoms (c and d, respectively). a, b: experimental, in transmission mode, c, d: generated for model sites in Figure 4a and b using FEFF [10].

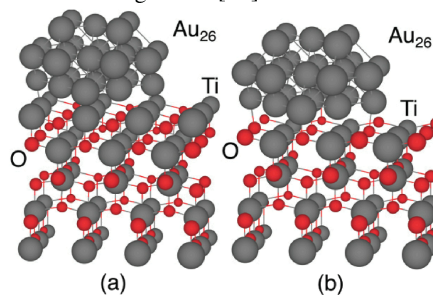


FIGURE 4. Au cluster models on anatase TiO₂(001) surface terminated with Ti atoms (a) and O atoms (b).

Sn Site Identification for Pt-Sn/SiO₂ Catalyst

With the excitation energy set at 29235.0 eV, the Sn K α_1 emission peak for Pt-Sn/SiO₂ appeared at 25270.1 eV, shifted by -1.2 eV from that for Sn metal. The Sn K α_1 -detecting XANES spectrum was obtained (Figure 5a) by tuning the fluorescence spectrometer to 25270.1 eV.

An intense peak above the absorption edge appeared at 29206.3 eV, between 29204.9 eV for Sn^{II}O and 29209.3 eV for Sn^{IV}O₂. The corresponding peak for Sn metal (29201.7 eV) shifted to 29208.3 eV in theoretical XANES generated using FEFF8.1 [9] for a Sn atom model buried in Pt particles, suggesting electron transfer from Sn to neighboring Pt atom(s). Among several Pt-Sn site uniform/mixture models [15], a Pt-Sn alloy model illustrated in Figure 5b and a mixture site model of Sn metal and SnO₂ (c) were found to be acceptable. Sn K-edge EXAFS analysis indicated the presence of Sn-metal bonds at 2.71 Å [6] significantly shorter than a typical Sn-Sn bond length (2.81 Å). Thus, the dispersed alloy nanoparticle model was concluded to be most plausible, rather than a metallic/oxidic Sn site for the Pt-Sn/SiO₂ catalyst.

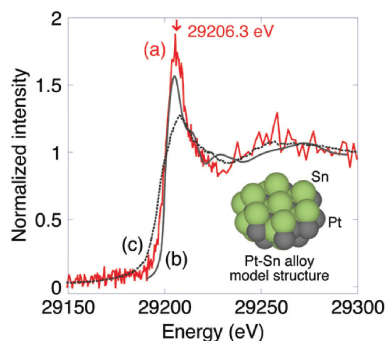


FIGURE 5. State-sensitive Sn K-edge XANES for Pt-Sn/SiO₂ catalyst (a). Spectrum generated using FEFF for the Pt-Sn alloy model (inset) (b). Average spectrum for Sn metal and SnO₂ (ratio 1:1) (c). Spectrum (c) was broader because the spectrum for SnO₂ was measured in transmission mode.

FUTURE PROSPECT

A more direct approach to study catalytic sites than state-sensitive studies is *frontier orbital-sensitive XAFS* by the discrimination of fluorescence lines due to the electron transition from a frontier orbital to a core hole. The feasibility was demonstrated for the physical mixture of V^{IV} and V^V compounds (Figure 6). Tuned to the energy of K β_5 for the V^{IV} site (5459.0 eV), the V^{IV} state was extracted and the 1s \rightarrow 3d pre-edge peak at 5468.2 eV was enhanced due to resonance excitation effects. The density of states near the Fermi level seems to consist significantly of V 3d because the V K

absorption edge structure resembled conventional spectrum for V^{IV}. In this way, V 3d frontier orbital-sensitive insights of V+TiO₂ catalysts will be given under on-site conditions of catalytic ethanol dehydration under visible light [16].

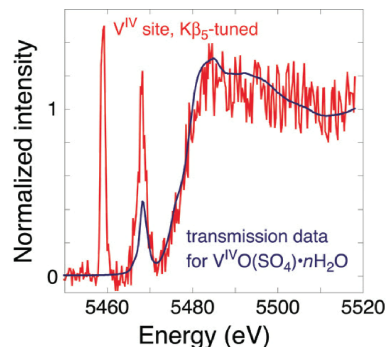


FIGURE 6. V K-edge XANES tuned to 5459.0 eV for a physical mixture of V^{IV}O(SO₄) \cdot nH₂O and Na₃V^VO₄ (1:1) (Red/Gray) and for V^{IV}O(SO₄) \cdot nH₂O measured in transmission mode (Blue/Black).

ACKNOWLEDGMENTS

This work was supported from the Grant-in-Aid for Scientific Research (C17550073) and the Priority Area "Molecular Nano Dynamics" (432-17034013) from MEXT. X-ray experiments were performed under the approval of the SPring-8 Program Review Committee (2006A1156, 2004A0122, and 2003B0386) and that of PF Proposal Review Committee (2005P014).

REFERENCES

1. F. W. F. de Groot, *Top. Catal.* **10**, 179 – 186 (2000).
2. Y. Izumi, *et al.*, *J. Electron Spectrosc. Relat. Phenom.* **119**, 193 – 199 (2001).
3. A. Cho, *Science* **299**, 1684 – 1685 (2003); A. T. Bell, *ibid.* **299**, 1688 – 1691 (2003).
4. G. R. Bamwenda, S. Tsubota, T. Nakamura, and M. Haruta, *Catal. Lett.* **44**, 83 – 87 (1997).
5. H. Yoshitake, T. Sugihara, and T. Tatsumi, *Chem. Mater.* **14**, 1023 – 1029 (2002).
6. Y. Izumi, T. Uruga, *et al.*, *Anal. Chem.* **77**, 6969 – 6975 (2005); *ibid.* **78**, 2075 (2006).
7. A. Krolzig, G. Materlik, M. Swars, and J. Zegenhagen, *Nucl. Instr. Meth.* **219**, 430 – 434 (1984).
8. R. W. Alkire, G. Rosenbaum, and G. Evans, *J. Synchrotron Radiat.* **7**, 61 – 68 (2000).
9. M. O. Krause and J. H. Oliver, *J. Phys. Chem. Ref. Data* **10**, 329 – 338 (1979).
10. A. L. Ankudinov, B. Raval, J. J. Rehr, and S. D. Conradson, *Phys. Rev. B* **58**, 7565 – 7576 (1998).
11. M. S. Chen *et al.*, *Science* **306**, 252 – 255 (2004).
12. E. D. Park and J. S. Lee, *J. Catal.* **186**, 1 – 11 (1999).
13. M. Valden, *et al.*, *Science* **281**, 1647 – 1650 (1998).
14. D. B. Akokekar, G. Foran, and S. K. Bhargava, *J. Synchrotron Radiat.* **11**, 284 – 290 (2004).
15. Y. Izumi, D. Masih, E. Roisin, J. P. Candy, H. Tanida, and T. Uruga, *Mater. Lett.*, in reviewing process.
16. D. Masih, H. Yoshitake, and Y. Izumi, *Appl. Catal. A*, in reviewing process.